RSC Advances

RSC Publishing

PAPER

View Article Online
View Journal | View Issue

Cite this: *RSC Advances*, 2013, **3**, 17515

Exploring the role of varied-length spacers in charge transfer: a theoretical investigation on pyrimidine-bridged porphyrin dyes†

Meiyuan Guo,[a] Ming Li,[ab] Yulan Dai,[a] Wei Shen,[a] Jingdong Peng,[a] Chaoyuan Zhu,[c] Sheng Hsien Lin[c] and Rongxing He*[ab]

Received 8th February 2013,
Accepted 20th July 2013

DOI: 10.1039/c3ra40702k

www.rsc.org/advances

A series of dyes based on a porphyrin donor and a cyanoacrylic acid anchor/acceptor group for solar cell application are investigated with regards to varied-length π-spacers affecting the photo-to-electric conversion efficiency (PCE). Investigations are firstly performed on three porphyrin sensitizers with 1–3 conjugated phenylethynyl (PE) units, which have experimentally proved that the efficiency of power conversion decreases systematically with increasing spacer length. The distances and amounts of charge transfer after photoexcitation are calculated. In the PE bridged porphyrin dyes, the calculated electron injection driving forces and the regeneration driving forces gradually decrease as the distance of the π-spacer increases. Our theoretical calculations can reproduce well the experimental conclusion, showing that the photo-to-electric efficiency has a strong distance dependence for the electron-rich phenyl spacer. Then we replace the phenyl group with a pyrimidyl (PM) group to uncover how the characteristics of the π-spacer affect the performance of optical absorption, charge separation, and the regeneration process, to further improve the power conversion. We find that the adoption of electron-deficient pyrimidyl can break and even remove the distance dependence of the π-spacer. Some integral factors affecting the dye performance, such as short-circuit photocurrent, open-circuit voltage and charge collection efficiency are analyzed. It would help to interpret what role the electron deficient π-spacers with varied lengths will play and how they are expected to behave in the performance of sensitizers. In this regard, this study presents us with a promising way to design novel functional dyes and to utilize the potential advantages of the lengthy spacer dyes.

1. Introduction

Following the much-cited *Nature* paper published by O'Regan and Grätzel[1], the past few decades have witnessed an increasing popularity in dye-sensitized solar cells (DSSCs) research.[2] People may expect that the increase in effort has led to a great improvement in the photo-to-electric conversion efficiency (PCE) of DSSCs. Green and co-workers have collated the PCE in various solar cells, and their work shows that the efficiency progress has slowed down in the past few years.[3] In nanocrystalline TiO_2 based DSSCs, a PCE conversion efficiency up to 11.1% had been obtained using the so called black dyes, a ruthenium (Ru) dye co-adsorbed with deoxycholic acid under standard air mass (AM) 1.5 sunlight.[4] The limited absorption in the near infrared region (NIR) of the solar spectrum, together with their undesirable environmental impacts, have stimulated scientists to search for more excellent and safer dyes.[2] The porphyrin system exhibits intense spectral response bands in the visible region and even part of the near infrared region, possesses good chemical, optical and thermal stabilities, and provides good potential candidates for photovoltaic applications, which have provoked scientists' interest.[5–10] Grätzel and co-workers, in their pioneering work on porphyrin dye, reported a PCE value of 2.6%.[5] Most recently, Diau reported a series of porphyrin based sensitizers, in which the maximum efficiency has reached 12.3% through co-sensitization with another organic dye.[6–10] The boosted efficiency offers a good prospect for porphyrin dyes as photosensitizers in the DSSCs. It also draws to our attention the need to do some prepared work on porphyrin and to see how far it can be extended. In our previous work,[11,12] we have implemented

[a]*School of Chemistry and Chemical Engineering, Southwest University, Chongqing 400715, China. E-mail: hxpengjd@swu.edu.cn; herx@swu.edu.cn*
[b]*Education Ministry Key Laboratory on Luminescence and Real-Time Analysis, Southwest University, Chongqing 400715, China*
[c]*Department of Applied Chemistry, Institute of Molecular Science and Center for Interdisciplinary Molecular Science, National Chiao-Tung University, Hsinchu 300, Taiwan*

† Electronic supplementary information (ESI) available: Calculated transition energies, oscillator strength, and configurations of porphyrin sensitizers with TD-DFT method. Electron density difference plots of electronic transition for each porphyrin. Molecular orbitals involved in electron transitions. See DOI: 10.1039/c3ra40702k

comprehensive calculations on the electronic configuration and highly resolved optical spectra of porphyrin photosensitizers, and the results gave us an insight into their structural details and provided direction on how to readily manipulate porphyrins' electronic configuration through adjustment to their structures.

We here introduce three elementary steps which sensitizers directly participate in during operation of DSSCs. In this study, modifications on porphyrin are made on the basis of property changes associated with the three steps. Firstly, upon photoexcitation of light in visible-NIR, the sensitizers are promoted to an electronic excited state. It is the first step in the sequence of processes that lead to power generation in the DSSCs. So the light-harvesting efficiency, which ties to the spectral coverage and absorptivity, plays a key role in the PCE of sensitizers. Porphyrin is one of several leading sensitizers that can address both issues.[2,13] It has two major absorption bands: the Soret (B) band and the Q band. Symmetrical porphyrin has a strong absorption in the B band and a weak one in the Q band.[14–16] We can obtain red-shifted and strengthened Q bands through modification on the porphyrin structure, eventually becoming nearly as intense as the B bands. Secondly, electron injection from the excited sensitizers into the conduction band (CB) of the semiconductor happens subsequently. Intramolecular charge transfer transitions occur in this step, one charge injects into the bulk material and the other resides on the sensitizer, which represents a key step in the PEC process.[2,17,18] Towards a high PEC efficiency, a maximum charge separation is highly desirable.[2,19–21] Thirdly, oxidized sensitizers are regenerated by a reducing agent of the electrolyte (such as I^-).[22,23] The regeneration efficiency plays an important role in the continuous circulation of electron transport, the overall electron transport motion giving rise to the macroscopic photocurrent.[2,18] Here, we are concerned with influences of the π-spacer length upon the above mentioned processes and further upon the PCE. The design of a new sensitizer which combines favorable spectral coverage and absorptivity with favorable charge separation is a key issue in the development and optimization of dye-sensitized solar cells. The charge separation process in such dye-sensitized films is based on electron injection from the excited state of the dye into the conduction band of TiO_2 after photoexcitation. The π-spacer should not be considered a bit part in the conversion process, but rather it plays a crucial role in tuning the main properties of the dye as sensitizer. Understanding how and why different chemical modifications in the conjugated link tune the electronic structure of the sensitizer should guide future computational and experimental studies to keep improving the PCE of organic dyes.

Diau and co-workers synthesized a category of zinc porphyrins with 1–3 conjugated phenylethynyl (PE) units as a link of controlled length.[6] When these porphyrins were fabricated into DSSC devices, they indicated that the PCE of these devices decreased systematically with increasing length of the link. In their following work,[7] they implemented supplementary research on these porphyrins to interpret this phenomenon. They found that the values of the short circuit photocurrent (J_{sc}) and open circuit voltage (V_{oc}), two main parameters affecting the PCE, decreased systematically with the increasing link. Albinsson and co-workers studied the charge injection and recombination kinetics of a series of triphenylamine based dyes for solar cell sensitization with different conjugation lengths.[24] They found that the incident photon to current conversion efficiency (IPCE), which is closely related to the driving force of charge injection, decreased with increasing conjugation length. Also, the recombination kinetics were exponentially dependent on the electron transfer distance in accordance with a super-exchange interaction between the electrons in the CB and the oxidized dye, the shortest dye giving the largest fraction of slowly decaying component.

Besides organic sensitizers, the effect of changing the electron transfer distance has also been investigated for a few ruthenium complexes,[25–27] all showing varied distance dependence. Interestingly, they all chose phenyl as the π-spacer unit to consider the effect of spatial separation on electron transfer dynamics with one accord. In these works, increasing the distance has side effects of slowing the electron injection rate, decreasing the V_{oc} and J_{sc} and further deteriorating the performance of the sensitizers. In our previous work,[28] we have suggested that adoption of the electron deficient pyrimidine as π-spacer could make for a higher light harvesting efficiency, more advantageous regeneration of oxidized dye, more effective unidirectional electron movements, and further obtain a higher conversion efficiency value, compared with the adoption of phenyl. We here built a preliminary series of pyrimidyl bridged porphyrin sensitizers with varied lengths, aimed at the design of all-round lengthy π-spacer sensitizers with high electron injection efficiency, good light-harvesting efficiency, and a favorable regeneration process of the oxidized dye. Besides, increasing the length of the bridge can provide more space for structural modifications, and the increase of volume can also hinder the aggregation of dyes. However, the adoption of an electron-rich π-spacer in long bridged dyes shows low electron injection efficiency because of the lack of electron driving force,[24–26] though they can reap strong and red shifted optical absorption. From the experimental point of view, the syntheses of such all-sided sensitizers are extremely demanding. Therefore, we would like to predict beforehand the potential properties of possible candidates in order to screen out molecules without the desired qualities and find those systems worth testing experimentally.

2. Computational details

It is worth pointing out that the density functional theory (DFT) method and time-dependent DFT (TD-DFT) can provide an improved treatment of the electron correlation effects and as a result, show good agreement with the experimental results.[29–33] The main purpose of the Kohn–Sham molecular

orbitals (MOs) of DFT is to represent the one-electron density.[34] In contrast to Kohn–Sham MOs, Hartree–Fock (HF) orbitals have well-defined chemical interpretations: frontier orbitals are used to describe chemical reactivity, and orbital energies are related to excitation energies *via* Koopman's theorem. The simple HF ground state Hamiltonian is replaced in TD-DFT by sophisticated DFT functionals that take electron correlation into account. As extensively discussed in Rosa's work,[35] the Kohn–Sham orbital model is very suitable for interpretation of the electronic structure and elucidation of the character of the excitations. They are thus used routinely to provide a useful tool for qualitative analysis of chemical properties.[36] The electronic structures of ruthenium dyes,[37,38] TiO_2 solids,[39] and nanocrystals[40], as well as dye-sensitized TiO_2,[41] have all been successfully analyzed in this way.

In this present work, full geometry optimizations and electronic structure calculations of porphyrin sensitizers were performed in tetrahydrofuran (THF) solvent using the polarized continuum model (PCM) with B3LYP functional and 6-311G(d,p) basis set. The functional B3LYP has an empirically determined contribution ($\sim$20%) of the nonlocal HF exchange term and, typically, shows excellent agreement with experiment. In order to validate the calculation results with the B3LYP functional, the transition energies of the Q band and the B band absorption for compound 10,20-biphenylporphinato zinc(II) (ZnBPP) with 1–3 π-conjugated phenylethynyl (PE) units (labeled 1PE1, 2PE and 3PE) were computationally explored and compared to experimental results with TD-DFT (B3LYP, PBE0, CAM-B3LYP, LC-WPBE, M062X, and WB97XD functionals. For more details, see the ESI†). The discussions of functional dependence were provided by Dreuw, Jacquemin, and Casanova *et al.*[42–46] They concluded that the long-range hybrids would be superior to the conventional hybrids. But here the best TD-DFT results were obtained by the B3LYP functional. Reasonable S_0–S_1 transition energies could also be obtained with the WB97XD functional, but it failed in the B band absorption calculations. Besides, transition energy dependence on the molecular geometry has been explored using the WB97XD optimization approach, and we found that better results were obtained when ground state geometries were optimized by the B3LYP functional. The use of WB97XD geometries leads to overestimation of the energy gaps. Electron density difference plots, electron transfer distance and the fraction of electron exchange were calculated. Interestingly, it even offered us improper fractions of electron exchange, the fractions were decreased with the increasing length of spacer, although they lingered around an approximate value. As we know, with the extension of a rich-electron spacer, the extended spacer could arouse the probabilities of electron movement from donor to acceptor, and then the fractions should be increased with increasing bridge length. In conclusion, the results calculated with the B3LYP functional in our work are reasonable, although there are some little deviations, but all calculations were performed at the same level and reproduced the experimental results. Frequency calculations at the same level were performed to confirm each stationary point to be a true energy minimum. In order to calculate the redox potentials, based on the Born-Haber cycle, the geometries of the mono-valent and bi-valent oxidized porphyrin sensitizers in THF solvent were also optimized using the B3LYP/6-311G(d,p) level. All redox potentials involved in this study were obtained *versus* the normal hydrogen electrode (NHE).[2] The electronic absorption spectra of sensitizers were calculated with the TD-DFT method in THF solvent.

Furthermore, the electron density differences were calculated and compared for screening of the sensitizer candidates for DSSCs with effective charge separation.[28] The plots gave a clear vision of electron movement after photoexcitation. The electron densities of all orbitals that related to the electron transitions were calculated with code *Multwfn 2.5*.[47] In order to investigate the PCE dependence on the length of the π-spacer, we calculated the distance of charge transfer and the fraction of charge exchange, which are linked to a specific photoexcitation transition. The quantifying calculations could present a more convincing result along with previous calculations. The distance and fraction were calculated with *DctViaCube*.[48]

These above-mentioned calculations were implemented to achieve insights into the geometrical and electronic structures of the varied-length porphyrin dyes and to bring up the structural modifications required to optimize the properties of the porphyrins based DSSCs. All DFT and TD-DFT calculations were performed using the Gaussian 09 program.[49]

3. Results and discussion

Considerable attention was paid to increasing the light harvesting efficiency, such as extending the coverage of optical absorption and enhancing the absorptivity.[2] It is important to find the relationship between the molecular as well as electronic structures of the porphyrin sensitizers and the photo-to-electric conversion performances of corresponding solar cells. In addition to acquiring a good spectral coverage and absorptivity of visible to near-infrared light, there should be a large enough driving force to guarantee efficient electron injection, while the ground state oxidation potential of dyes should match the semiconductor and the redox couple (I^-/I_3^-) to ensure optimal regeneration of the oxidized dye.[2,17,22,23] Usually, in order to obtain an intimate electronic coupling for the charge injection between the dye and the semiconductor, a suitable anchoring group should be assembled to strongly adsorb onto the semiconductor surface.[17,18] As a result, to satisfy these requirements, we here adopted zinc porphyrin and 2-cyanoacrylic acid to build the donor–π–acceptor (D–π–A) structural motif.

As we know, the overall photo-to-electric efficiency, η, is closely connected with the short-circuit current density, J_{sc}, the open-circuit photovoltage, V_{oc}, and the fill factor, FF, and the relationship is expressed as:[13,32]

$$\eta \equiv \frac{J_{sc} \cdot V_{oc} \cdot FF}{P_{in}} \quad (1)$$

P_{in} is the total solar power incident on the cell, 100 mW cm^{-2} for AM 1.5. So, the most straightforward way to improve the PCE, η, is to increase J_{sc}, V_{oc}, and FF. The FF depends on the diode quality factor (γ) and the open-circuit photovoltage (V_{oc}). Generally, a higher FF value could be acquired with a smaller γ and a larger V_{oc}. Typical values for the FF range from 0.75 to 0.85.[13] There is thus little space for optimization and improvement of the FF and it won't be considered further here. In this paper, we mainly investigate how various integral factors, such as the efficiencies of light harvesting, electron injection, oxidized dye regeneration, and charge separation affect the J_{sc} and V_{oc}, and further affect η.

Parallel comparisons between electron-rich phenyl bridged and electron-deficient pyrimidyl bridged sensitizers are carried out, which aim to prove that the adoption of electron-deficient pyrimidyl can break and even remove the distance dependence of π-spacer, and further improve the dye performance through prolonging the length of π-spacer. It presents us with a promising way to utilize the advantages of the lengthy bridged dyes. These studies helped us to find out the relationship between the molecular electronic structure of porphyrin sensitizer and the performance of the porphyrin-sensitized solar cells, and brought to light how the photophysical properties play the key role in DSSC efficiency.

3.1 Electronic structure and spectra

Based on the previous experimental and theoretical results, we firstly performed our calculations on three synthesized porphyrins, ZnBPP-1PE, ZnBPP-2PE, and ZnBPP-3PE. ZnBPP acts as a light harvesting center (and also as a donor group),[6] see Fig. 1, which possesses a stability against irradiation and facilitates the synthesizing and improving of the chemical structures (hence their electrochemical and photochemical properties). The consistency between experimental results and our theoretical ones gives us sufficient confidence to modify and design novel porphyrin sensitizers, and to uncover the superiority of electron deficient π-spacers in improving the performance of sensitizers. In this work, we designed six novel pyrimidyl bridged porphyrin sensitizers to investigate the roles of length and character of spacer in DSSCs' performance. The optimized molecular frames are presented in Fig. 1. From a geometrical point of view, density functional calculations of the molecules mentioned above show a coplanar conformation between the zinc porphyrin moiety and the π-spacer connect-

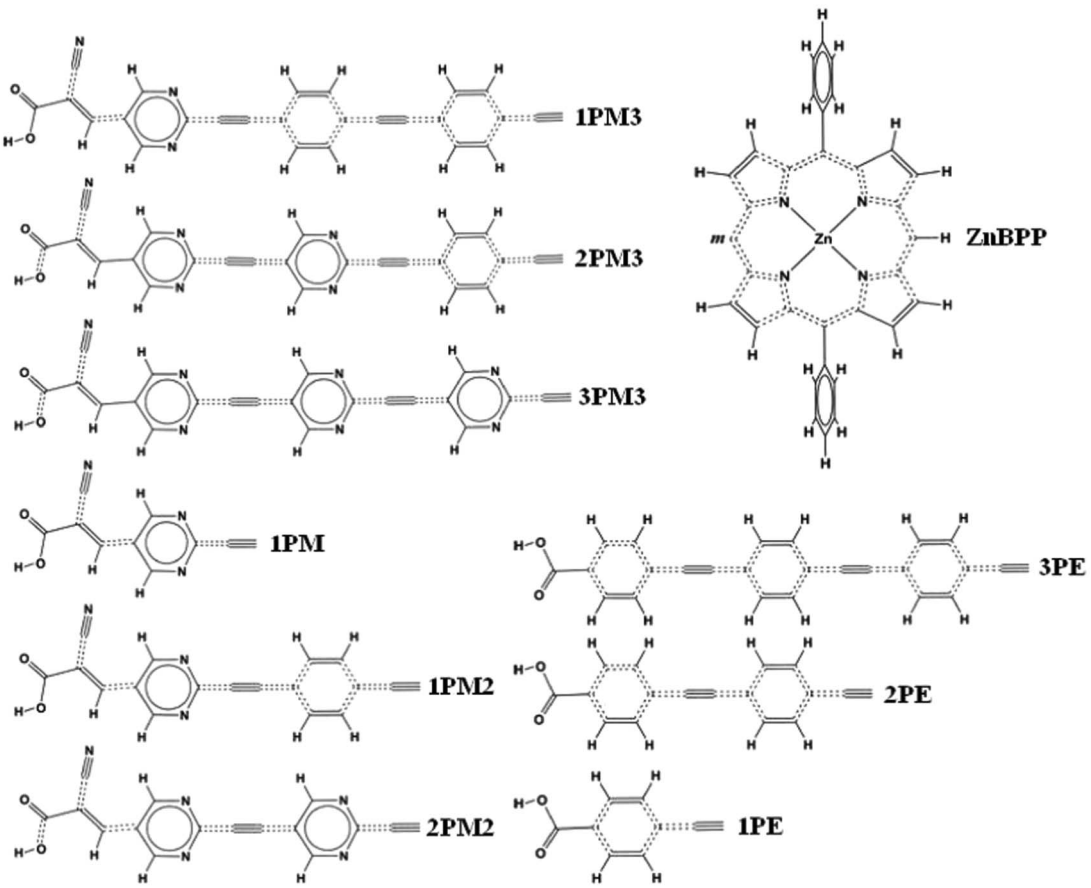

Fig. 1 Schematic diagram of phenyl and pyrimidyl bridged porphyrins, these spacers combined to anchoring groups are attached on the *m* point on the ZnBPP moiety.

Table 1 Calculated HOMO, LUMO, and fragment (F) LUMO energy levels (eV) for porphyrin sensitizers and the length of π-spacer (*L*) (Å)

Schemes	1PE	2PE	3PE	1PM	1PM2	2PM2	1PM3	2PM3	3PM3
HOMO	−5.334	−5.273	−5.252	−5.519	−5.530	−5.470	−5.273	−5.311	−5.454
LUMO	−2.858	−2.856	−2.853	−3.369	−3.381	−3.485	−3.392	−3.505	−3.549
F-LUMO	−2.630	−2.807	−2.850	−3.696	−3.574	−3.736	−3.496	−3.611	−3.773
L	6.861	13.734	20.593	6.741	13.610	13.476	20.477	20.348	20.200

ing anchoring group. The coplanar push–pull system is favorable due to the interaction between the electron donor group (EDG) and the conjugated π-spacer. Furthermore, it is beneficial to the electron injection due to the modified appropriate energy level arising from introduction of the π-conjugated spacer. The measured phenylethynyl and pyrimidinylethnyl lengths are available in Table 1, as due to the near planarity, the length of π-spacer can be measured from the distance between two terminal points.

The extension of phenylethynyl hardly introduces an impact on the lowest unoccupied molecular orbital (LUMO) energy levels, and the results are −2.858 eV, −2.856 eV, and −2.853 eV for ZnBPP-1PE, ZnBPP-2PE, and ZnBPP-3PE, respectively. It corresponds well with Diau and co-workers' results.[6] For pyrimidyl bridged porphyrin sensitizers, the values of the LUMO energy levels are −3.369 eV, −3.485 eV, and −3.549 eV for ZnBPP-1PM, ZnBPP-2PM2, and ZnBPP-3PM3, respectively. Comparing ZnBPP-1PE with ZnBPP-1PM, we concluded that the replacement of phenyl units with pyrimidyl could well stabilize the LUMO energy, as the energy drop is about 0.6 eV. As an analogy of this result, we found that in pyrimidyl bridged porphyrin sensitizers, the LUMO energies are stabilized with increasing π-spacer length and the number of pyrimidyl units (Fig. 2). Specifically, the cyanoacrylic acid can also stable the LUMO energy, which we have indicated in our previous work. The role of cyanoacrylic acid and carboxylic acid anchoring groups were analyzed and compared in detail by designing novel sensitizers which had the phenyl unit combined with a cyanoacrylic acid moiety, and the pyrimidyl unit connected with a carboxylic acid group.[28] Compared with the dramatic drop of the LUMO energy, the replacement has a relatively minor effect on the HOMO energy level. Interestingly, the HOMO energies systematically increased with increasing length of pyrimidyl bridged spacer, although the change is small. The values are −5.519, −5.470, and −5.454 eV for ZnBPP-1PM, ZnBPP-2PM2, and ZnBPP-3PM3, respectively. They are still much lower than the phenyl bridged values. The HOMO energy destabilization would result in the sensitizers being prone to oxidation and hence be sensitive to air, that is to say, the pyrimidyl bridged porphyrins possess better stability against irradiation than phenyl bridged dyes. Generally, the Q band is derived from the HOMO to the LUMO, which is the major contribution for electron transition from the ground state (S_0) to the first excited state (S_1) (see Table S1 in ESI†). This behavior is also confirmed by the good linear relationship between the transition energies, and the HOMO to LUMO energy differences. Comparing pyrimidyl bridged porphyrins with phenyl ones, the differential drop value narrows the energy gap between LUMO and HOMO, thereby making it possible to shift the Q bands to longer wavelengths. Except for the advantage of shifting the optical absorption band by tuning the orbital energy levels, the extension of the pyrimidyl spacer could also make for favorable electron transfer. In a simplified orbital description of electron transfer, the electron can be visualized as moving from the LUMO of ZnBPP to the LUMO of the semiconductor, tunneling through the LUMO of the conjugated π-bridge. So here we separately calculated the energy levels of acceptor fragments (anchoring group and conjugated π-spacer) and donor group (ZnBPP) of the sensitizers. Obviously, the LUMO energy levels of fragments for pyrimidyl bridged porphyrins are in the order of 1PM (−3.696 eV) > 2PM2 (−3.736 eV) > 3PM3 (−3.773 eV).

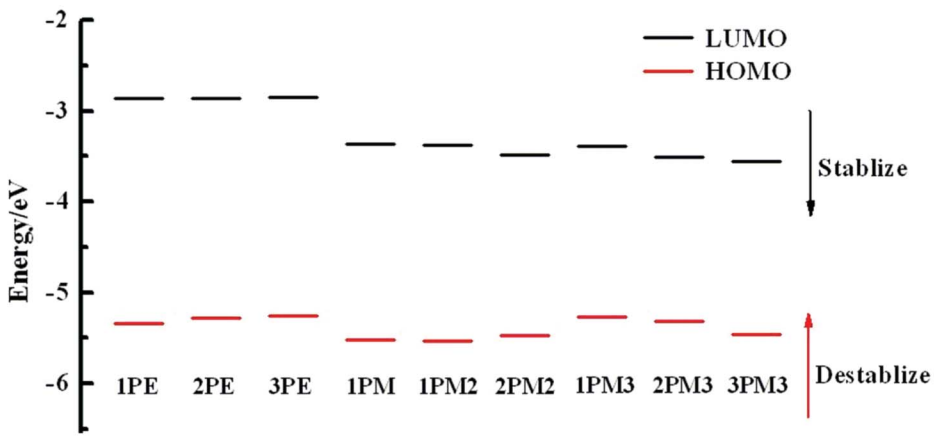

Fig. 2 Energy-level diagram of phenyl and pyrimidyl bridged porphyrins showing the HOMO (red) and the LUMO (black) of each porphyrin.

The levels dropped dramatically compared with phenyl bridged ones, they are 1PE (−2.630 eV) > 2PE (−2.807 eV) > 3PE (−2.850 eV). All of them are located below the LUMO energy level of the ZnBPP moiety (−2.539 eV). The energy drops of $LUMO_{donor}-LUMO_{acceptor}$ comply with the sequence of 3PM3 (1.234 eV) > 2PM2 (1.197 eV) > 1PM (1.157 eV) > PE3 (0.311 eV) > PE2 (0.268 eV) > PE1 (0.091 eV). Also, we find that the drops would be larger with increasing the number of pyrimidyl units, 2PM2 (1.197 eV) > 1PM2 (1.035 eV) and 3PM3 (1.234 eV) > 2PM3 (1.072 eV) > 1PM3 (0.957 eV), which indicate that the adoption of pyrimidine is favorable for charge separation between the ZnBPP and the extended substituent. The position of the LUMO level and the nature of the acceptor group play an important role in determining the electronic coupling and therefore the efficiency of electron injection. A telling example is ruthenium bipyridine dyes,[1] where carboxylates have been proved to be favorable to electron injection by decreasing the LUMO energy of the bipyridine unit attached to the carboxylates, thereby ensuring the LUMO orbital of the dye is localized upon the bipyridine unit closest to the metal oxide surface.

With the indication of structural modification affecting the orbital energy levels, we could acquire much more red-shifted optical absorption. The simulated absorption spectra are presented in Fig. 3. The upper one is the optical absorption spectra of phenyl bridged porphyrins, evidently, exhibiting two major absorption bands: short wavelength Soret (B) bands and longer wavelength Q bands, which are located around 400 nm and 600 nm, respectively. There is an absorption vacancy between the B and Q bands. For the Q band, as the extension just has a slight influence on the LUMO and HOMO energy levels, so the Q bands of phenyl bridged porphyrins are nearly situated around the same position, they are 591, 604 and 609 nm for ZnBPP-1PE, ZnBPP-2PE, and ZnBPP-3PE, respectively. The oscillator strengths (f) of the Q bands are enhanced with increasing π-spacer length: they are 0.382, 0.778, and 1.057, separately. On the contrary, the strengths of the B band decreased with increasing length: they are 1.659, 1.362, and 1.126 for ZnBPP-1PE, ZnBPP-2PE, and ZnBPP-3PE. The extension weakens the absorption in the B region, but more moderately strong bands appear in the left side of the B region, which contribute to the overall optical absorption coverage. The bottom part in Fig. 3 is the optical absorption spectra of pyrimidyl bridged porphyrins. Compared with the phenyl bridged ones, one of the most remarkable features is the red-shifted Q bands. They are approximately situated in the range from 660 to 760 nm because of the sharp drops of the LUMO energy levels and the optical absorptions in the Q region are stronger than for the phenyl bridged porphyrins except the longest one. For ZnBPP-3PM3, there are three bands with oscillator strengths larger than 1.0, although the absorption in the Q band region is slightly smaller. Besides, there are new absorption bands between the B bands and Q bands for pyrimidyl porphyrins. The bathochromic shift of the Q bands and the fill in of the optical absorption vacancy can largely improve the light harvesting efficiency (LHE). The LHE can be expressed as:[32,50]

$$\varphi_{LHE} = 1 - 10^{-f} \quad (2)$$

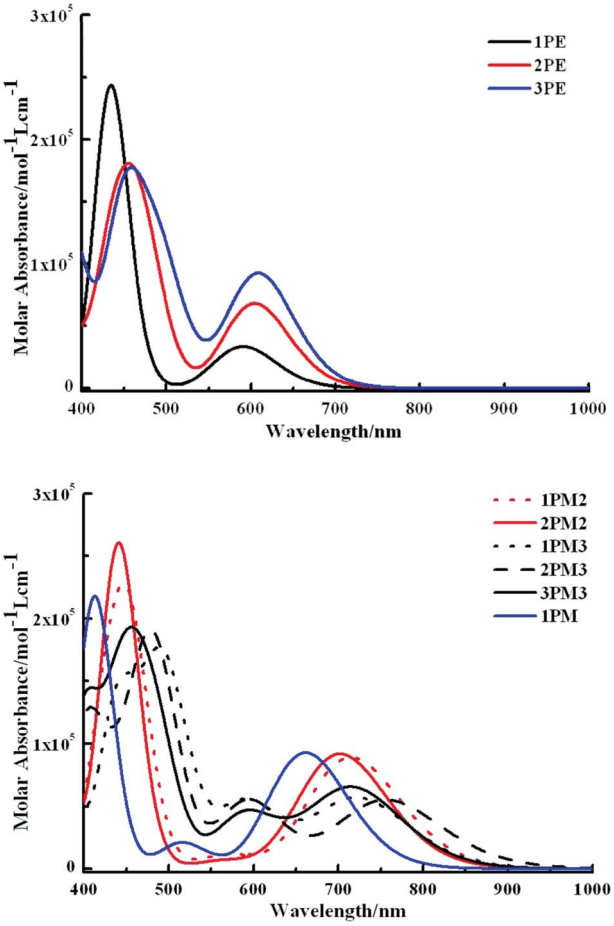

Fig. 3 Simulated optical absorption spectra for phenyl bridged porphyrins (upper) and pyrimidyl bridged porphyrins (below). HWHM = 2500 cm^{-1}.

where f is the oscillator strength of the dye associated with a certain wavelength (λ). We have collected the φ_{LHE} in the Q region ($\varphi_{LHE(Q)}$), and the overall average light harvesting efficiency ($\varphi_{LHE(Aver)}$), these data are available in Table 2. Obviously, the fully pyrimidyl-conjugated porphyrins are superior to the phenyl-conjugated ones in terms of the $\varphi_{LHE(Aver)}$. The lowest $\varphi_{LHE(Aver)}$ in pyrimidyl-bridged porphyrin occurs with ZnBPP-1PM, however, the value of 0.680 is even larger than the highest one of 0.658 for the phenyl-bridged

Table 2 Calculated light harvesting efficiency (LHE) in the Q band region ($\varphi_{LHE(Q)}$), overall average LHE ($\varphi_{LHE(Aver)}$), the charge transfer distance (Å), electron exchange fraction (|e$^-$|), driving force (D) (eV), regeneration force (R) for the S_0–S_1 transition

Schemes	1PE	2PE	3PE	1PM	1PM2	2PM2	1PM3	2PM3	3PM3
E_{redox}	1.586	1.472	1.370	1.894	1.749	1.867	1.639	1.736	1.852
$\varphi_{LHE(Q)}$	0.585	0.833	0.912	0.910	0.905	0.911	0.774	0.767	0.818
$\varphi_{LHE(Acer)}$	0.658	0.626	0.631	0.680	0.593	0.763	0.586	0.713	0.708
Distance	2.141	2.924	3.818	8.038	15.076	14.632	21.219	20.749	20.343
Fraction	0.656	0.705	0.722	1.049	1.309	1.321	1.416	1.410	1.383
D	0.123	0.057	0.017	0.463	0.459	0.547	0.369	0.536	0.562
R	0.594	0.533	0.512	0.779	0.590	0.730	0.532	0.571	0.714

porphyrins. Most importantly, the structures we present are just prototypes. There is significant room for meliorating the zinc porphyrin structure and further improving the φ_{LHE} The φ_{LHE} of the dye has to be as high as possible to maximize the J_{sc}. The J_{sc} can be written as:[2,32]

$$J_{sc} = \int_{\lambda} \varphi_{LHE(\lambda)} \varphi_{inject} \varphi_{CC} d\lambda \quad (3)$$

where J_{sc} is a function of $\varphi_{LHE(\lambda)}$ (the light harvesting efficiency at a given wavelength), the electron injection efficiency (φ_{inject}) and the charge collection efficiency (φ_{CC}). It is hard to quantify the φ_{CC} theoretically, and intensity modulated photovoltage spectroscopy (IMVS) and intensity modulated photocurrent spectroscopy (IMPS) are used to evaluate the (φ_{CC}) of the DSSCs experimentally.[51] But here we confidently express that the extension of spacer would increase the φ_{CC}. Firstly, there is lots of evidence that prove that the recombination kinetics are exponentially dependent on the link length, *i.e.* the increase of link length could slow the electron recombination rates,[7,24–27] that is to say, further elevate the φ_{CC}. Secondly, the better the charge separation we obtain, the higher the φ_{CC} would be. A long pyrimidyl-bridged spacer would increase the efficiency of charge separation, thus increasing the φ_{CC}.[2] We discuss the charge separation in the following section. As a result, the enhancement of J_{sc} should focus on improving φ_{CC}, $\varphi_{LHE(\lambda)}$ and φ_{inject}. Specifically, the improvement of φ_{inject} not only contributes greatly to the J_{sc}, but also benefits the V_{oc}.[2,13]

3.2 Performance of photoinduced charge transfer characters

For most of the conjugated compounds, the excitation process often induces an intramolecular charge transfer transition and further leads to charge separation. One charge injects into the bulk material and the other resides on the sensitizer, for a typical donor–π-spacer–acceptor (D–π–A) sensitizer, it could be simply described as from a D–π–A ground state to a D^+–π–A^- excited state.[2,52] To address the optimal energy levels in a paired donor/acceptor of light harvesting system, the optical excitation energy gaps of both the donor and the acceptor should be engineered to match the photon energy, as both can harvest photons and incur charge separation at the donor/acceptor interface.[17,18] Firstly, the excited-state level of the photosensitizer should be higher in energy than the conduction band edge of the semiconductor conduction band (CB), so that an efficient electron transfer process from the excited dye to the CB of the semiconductor can take place. This efficiency of the charge separation is central to the performance of dye-sensitized solar cells. Secondly, the oxidized state level of photosensitizer must be more positive than the oxidized potential of electrolyte in order to facilitate the regeneration of the oxidized dyes. For longer phenyl bridged dyes, suggestions were made that the limiting factor for charge injection was the lack of sufficient driving force for electron injection.[7,24–27] In order to reverse this situation, the electron deficient pyrimidyl is introduced. To obtain optimal electron injection, the redox potentials of the dyes should match the semiconductor, which is fundamentally important to the function of DSSCs. The value of φ_{inject} depends on the coupling between photosensitizer and semiconductor. Actually, the thermodynamic driving force (D) could reflect φ_{inject} related to the corresponding vertical excitation. The driving force (D) can be calculated by eqn (4):[28,53]

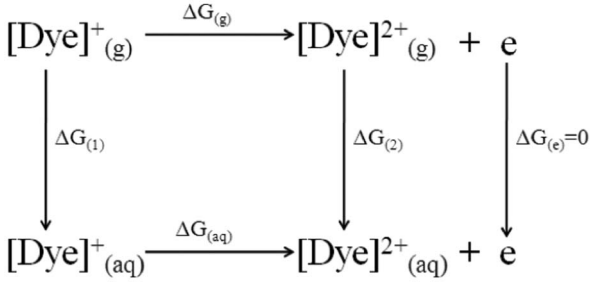

Scheme 1 Thermodynamic cycle used to calculate the redox potentials.

$$D = |E_{redox(dye)} - \Delta E - E_{CB}| \quad (4)$$

where ΔE is the vertical excitation energy which could be obtained from the TD-DFT calculation. The value of E_{CB} is the conduction band edge of TiO_2 (−0.44 V *vs.* NHE).[54] The redox potential of the system in the ground state, $E_{redox(dye)}$ *versus* normal hydrogen electrode (NHE) for a one-electron redox couple, is calculated through the Nernst equation and can be written in the energy scale as eqn (5):[53]

$$E_{redox(dye)} = \frac{\Delta G_{(aq)} - \Delta G_{(NHE)}}{nF} \quad (5)$$

The value of $\Delta G_{(aq)}$ is the Gibbs free energy change due to the oxidation of the dyes in solution. We can calculate it through the Born-Haber cycle, as shown in Scheme 1. $\Delta G_{(NHE)}$, the Gibbs free energy change of the normal hydrogen electrode, takes the standard value of −4.44 eV.[55] F denotes the Faraday constant (23.06 kcal mol^{-1} V^{-1}). n is the number of electrons involved in the redox couple $[dye]^{2+}/[dye]^+$ (here n = 1).

In the beginning, we calculated the electron injection driving forces of three phenyl bridged porphyrins, and the values were 0.123 eV, 0.057 eV, and 0.017 eV for ZnBPP-PE1, ZnBPP-PE2, and ZnBPP-PE3, respectively. The calculated results, presented in Table 2, reproduce well the experimental conclusion that the extension of π-spacer would decrease the driving force. In contrast, fully conjugated pyrimidyl bridged porphyrins show a reversed tendency, the order is ZnBPP-1PM (0.463 eV) < ZnBPP-2PM2 (0.547 eV) < ZnBPP-3PM3 (0.562 eV). Comparing ZnBPP-1PM2 with ZnBPP-2PM2, and analogically, comparing ZnBPP-1PM3 with ZnBPP-2PM3 and ZnBPP-3PM3, we can conclude that the π-spacer has a significant influence on $E_{redox(dye)}$ and further on the driving forces of electron injection. So the adoption and extension of pyrimidyl group would make for an advantageous electron injection process. In addition to the calculations of the values of driving forces for electron injection, the driving forces for regeneration are also calculated. The regeneration of the sensitizers is a key factor for maintaining the reuse of sensitizers, which could prolong the life expectancies of sensitizers.[2] Here the I^-/I_3^- redox couple is adopted. In order to engender an effective regeneration process, the dye oxidation potential should be

enough positive compared to the redox potential of the I^-/I_3^- electrolyte. Alebbi and co-workers reported that inefficient regeneration could limit the device photocurrent.[22] Their study focused upon a comparison of osmium and ruthenium based sensitizers. The osmium dye obtained a smaller ground state oxidation potential, resulting in the decrease of driving force for the regeneration, although it exhibited stronger near-infrared absorption. The lower photocurrent of the osmium based devices was assigned to slower iodide regeneration of the dye ground state. From the above discussion, we can get that the sensitizers combine the electron-deficient pyrimidyl have a vantage of generation of oxidized dyes. The regeneration driving forces are ZnBPP-1PE (0.594 eV) > ZnBPP-2PE (0.533 eV) > ZnBPP-3PE (0.512 eV). This tendency is in accord with pyrimidyl bridged porphyrins, ZnBPP-1PM (0.779 eV) > ZnBPP-2PM2 (0.730 eV) > ZnBPP-3PM3 (0.714 eV). The generation efficiency decreases with increasing π-spacer length, regardless of whether it is phenyl or pyrimidyl bridged. Specifically, the full conjugated pyrimidyl bridged ones hover at a higher level. This may be compared to 0.70 eV for the conventional N-719 complex (bis-(tetrabutylammonium)-*cis*-(dithiocyanato)-*N*,*N*′-bis(4-carboxylato-4′-carboxylicacid-2,2′-bipyridine)ruthenium(II)).[56] Besides, an anodic shift of the regeneration driving forces was observed with increasing number of pyrimidyl units, which could indicate that the electron deficient pyrimidyl group plays a positive role in improving the regeneration efficiency, though the extension would slightly weaken the effect.

Ideally, we expect that the electron is transferred from the donor part and localized on the acceptor part upon the excitation. But in most real cases, the transferred electron is delocalized from the region near to the donor to one in the vicinity of the acceptor, which varies the extent of charge separation. In order to inspect how varied-length spacers tune the charge transfer character, we here calculate the electron transfer distance and the fraction of electron exchange.[48,52] For the sake of implementing the calculations, the total electron density of initial and final states and then their centroids should be calculated. The total electron density difference ($\sum \partial_{\alpha\rightarrow\beta}$) after photoexcitation between the initial and final states could be expressed as the sum of all molecular orbital transitions involving each participating excitation α→β (α and β are denoted as the initial and final molecular orbitals, respectively):[28]

$$\partial_{\alpha\rightarrow\beta} = \frac{C^2_{\alpha\rightarrow\beta}}{\sum C^2_{\alpha\rightarrow\beta}}(\rho_\alpha - \rho_\beta) \quad (6)$$

$C_{\alpha\rightarrow\beta}$ is the orthogonal coefficient in the TD-DFT equation, and then $\frac{C^2_{\alpha\rightarrow\beta}}{\sum C^2_{\alpha\rightarrow\beta}}$ represents the contribution of the electron transition component to this absorption peak, ρ_α and ρ_β are the electron densities of the participating molecular orbital relative to the transitions. The electron density difference between initial and final states is the linear combination of various electron transition models. All these calculations could be performed with *cubman* utility provided by the Gaussian 09 and *Multwfn* programs. Subsequently, two functions $\rho_+(r)$ and $\rho_-(r)$ can be used for defining the increase and decrease of the density owing to the electronic transition. The centroids of spatial regions defined by $\rho_+(r)$ and $\rho_-(r)$, can be written as:[48]

$$C_+ = (x_+, y_+, z_+) = \frac{\int \vec{r}\rho_+(\vec{r})dr}{\int \rho_+(\vec{r})dr} \quad (7)$$

and

$$C_- = (x_-, y_-, z_-) = \frac{\int \vec{r}\rho_-(\vec{r})dr}{\int \rho_-(\vec{r})dr} \quad (8)$$

The distance of charge transfer can be defined as:

$$\text{Distance} = |C_+ - C_-| \quad (9)$$

The fraction of electron exchange can be expressed as:

$$\text{Fraction} = \int \rho_+(\vec{r})dr = \int \rho_-(\vec{r})dr \quad (10)$$

Based on the discussion of the above theoretical details, these parameters are calculated and the results are presented in Tables 3 and 4. Our purpose is to illustrate how the long pyrimidyl spacer affects the charge separation and the electron transfer process through modifying these energy and potential levels. These processes are important for improving the photo-to-electric efficiency of DSSCs. In the first instance, we shift our attention to the electron density difference plots for the lowest electron transitions, see Table 3. The calculated data in the first column showed that the fraction of electron exchange is increased with extension of the electron-rich phenyl group. The tendency is ZnBPP-1PE (0.656 e^-) < ZnBPP-2PE (0.705 e^-) < ZnBPP-3PE (0.722 e^-). The increase of bridge length in D–π–A sensitizers directly translates into greater π conjugation of the HOMO and LUMO and further increases the possibility of electron transfer from HOMO to LUMO, which would contribute to the enhancement of the fraction of electron exchange. In addition to the fraction, the overlap (denoted as *Ω*) between the regions of density depletion and increment are calculated. The extents of overlaps increase with the extension, $\Omega_{\text{ZnBPP-1PE}}$ (0.383) < $\Omega_{\text{ZnBPP-2PE}}$ (0.438) < $\Omega_{\text{ZnBPP-3PE}}$ (0.444). For a good charge separation, only a weak overlap should be evidenced. As we mentioned above, the charge separation plays an important role in determining the charge collection efficiency. For the phenyl bridged porphyrins, the extension of π-spacer would induce an adverse effect on the improvement of φ_{CC} in terms of the overlaps. For the calculated charge transfer distance (ΔD), they are 2.141 Å < 2.924 Å < 3.818 Å for ZnBPP-1PE, ZnBPP-2PE, and ZnBPP-3PE, separately. The ΔD is evidently less than their spacer lengths, 6.861 Å, 13.734 Å, and 20.593 Å. The transferred electron is still mostly delocalized around the attachment site between the ZnBPP and spacer. However, the optical absorption in the Q region is not weak, but the limited electron transfer performance would impair the availability in this region. It indicates that the sensitizer performance in dye-sensitized solar cells not only relies on the extrinsic spectral absorption intensity, but also depends on the intrinsic character of electron movement related to electron excitation. In this regard, we can conclude that the extension of the phenyl bridged spacer is unfavorable for the charge separation. For the pyrimidyl bridged porphyrins, the antici-

Table 3 Electron density difference plots of electronic transition $S_0 \rightarrow S_1$ for each porphyrin. $\Delta D$is the electron transfer distance (Å); $\Delta q$is the fraction of electron exchange ($|e^-|$), $\Omega$is the overlap between the regions of density depletion and increment. (Isovalue: 4×10^{-4} e au^{-3})

ZnBPP-1PE ΔD = 2.141, Δq = 0.656, Ω= 0.383	ZnBPP-1PM ΔD = 8.038, Δq = 1.049, Ω = 0.243	ZnBPP-1PM2 ΔD = 15.076, Δq = 1.309,Ω = 0.015
ZnBPP-2PE ΔD = 2.924, Δq = 0.705, Ω = 0.438	ZnBPP-2PM2 ΔD = 14.632, Δq = 1.321, Ω = 0.023	ZnBPP-1PM3 ΔD = 21.219, Δq = 1.416, Ω = 0.001
ZnBPP-3PE ΔD = 3.818, Δq = 0.722, Ω = 0.444	ZnBPP-3PM3 ΔD = 20.343, Δq = 1.383, Ω = 0.003	ZnBPP-2PM3 ΔD = 20.749, Δq = 1.410, Ω = 0.002

pated results are obtained. The fractions of electron exchange are ZnBPP-1PM (1.049 e^-) < ZnBPP-2PM2 (1.321 e^-) < ZnBPP-3PM (1.383 e^-). The ΔD is also increased with the extension of π-spacer, their values are 8.038 Å, 14.632 Å, and 20.343 Å, which are approximately consistent with the lengths of link, 6.741 Å, 13.746 Å, and 20.477 Å, and it means that increased length of π-spacer would not affect the charge transfer distances for pyrimidyl bridged porphyrins. A strong through-space charge transfer is created. Compared with phenyl bridged ones, we find that the adoption and extension of pyrimidyl spacers could greatly contribute to the enhancement of the amount and distance of electron transfer. Besides, the systematic decrease of overlaps, $\Omega_{ZnBPP\text{-}1PM}$ (0.243) > $\Omega_{ZnBPP\text{-}2PM2}$ (0.023) > $\Omega_{ZnBPP\text{-}3PM3}$ (0.003), indicates the extension of the pyrimidyl spacer could facilitate the charge separation, which is contrary to the phenyl bridged ones. Through the analysis of the fractions of electron exchange, electron transfer distances, and overlaps involved in the lowest electron transition ($S_0 \rightarrow S_1$) for pyrimidyl and phenyl bridged porphyrin sensitizers, we can summarize that the extension of electron deficient pyrimidyl spacer is superior to phenyl bridged ones in charge separation and electron movement. In order to implement comprehensive comparisons, all the electronic transition models with oscillation strength larger than 0.1 are taken into account and the graphs are presented in Table 4. The charge difference plots can be found in the ESI† (Table S2). For the distances of charge transfer, the fully pyrimidyl-conjugated porphyrins keep all the values at high levels and the phenyl bridged ones are sharply bumped, which suggests that favorable electron transfer movement is obtained through the adoption of a pyrimidyl group. The most remarkable feature for the fractions of electron exchange, when comparing pyrimidyl and phenyl bridged ones, is the higher fractions can be acquired in the lowest energy transition region by pyrimidyl bridged porphyrins. We previously proved that the pyrimidyl spacer could allow for unidirectional electron movements (donor to acceptor), while the phenyl spacer would give rise to reversible electron movements.[28] Here, for the three phenyl bridged porphyrins, we also find reversible electron movements at 341.8 nm (f = 0.230), 368.1 nm (f = 0.516), and 453.9 nm (f = 1.127) for ZnBPP-1PE, ZnBPP-2PE, and ZnBPP-3PE, respectively (see ESI,† Table S2). We find that the LUMO+1, which acted as the final orbital in these three transitions, plays a major role in the reversible electron movement. Through the spatial distributions of molecular orbitals involved in electron transitions, the electron distribution of LUMO+1 is entirely located at the porphyrin circle (see ESI,† Table S3). The phenomenon of reversible electron movement is derived from the electron transitions to LUMO+1. The situation remained unchanged when the carboxylic acid group was replaced with a cyanoacrylic acid group in the phenyl based porphyrin

Table 4 Evolution of the main parameters for increasingly long chains. Left: charge transfer distance (Å). Right: fraction of exchange electron ($|e^-|$). Only the electronic transitions with oscillator strengths larger than 0.1 are taken into account. (Horizontal ordinate is the number of calculated electron transition states)

Charge transfer distance	Fraction of exchange electron
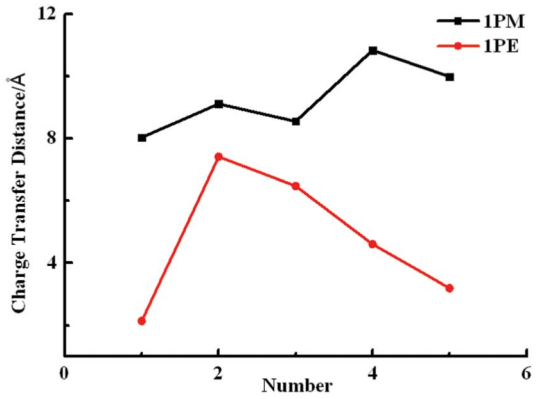	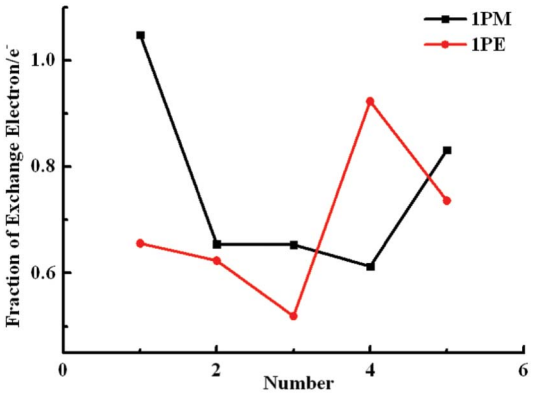
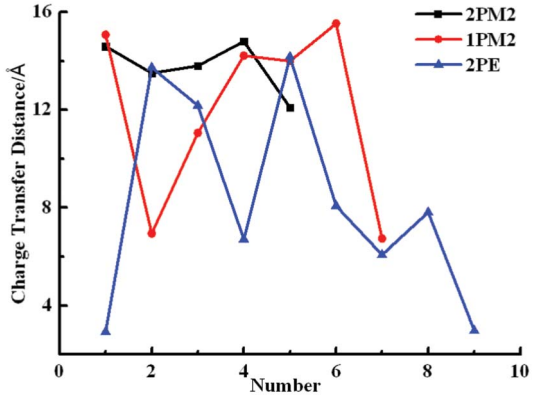	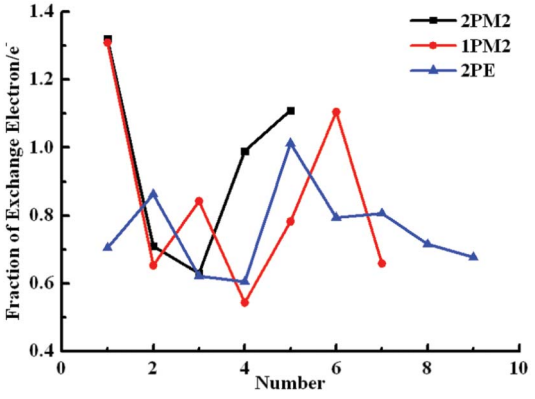
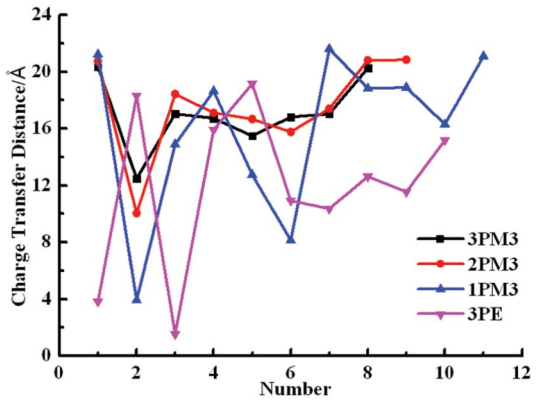	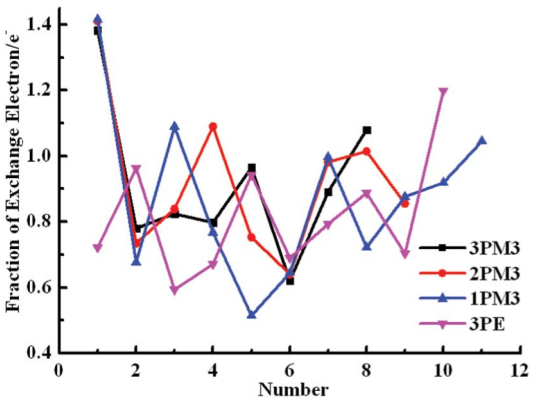

sensitizers.[28] From the comparison of the electron density difference plots of the sensitizers with and without the pyrimidine, we could conclude that the presence of electron deficient pyrimidine played a key role in the unidirectional electron movements. These results could be ascribed to the stronger coupling interaction between the donor group and the bridge, while the coupling between the anchoring group and bridge group is relatively smaller . In other words, there is a low energy barrier for electron transport from the donor to the acceptor tunneling through the bridge group and a relatively higher energy barrier for the reverse electron movements.[57–59] As reported by Wiberg and his co-workers, the coupling interaction difference could result in charge separation and unfavorable reversal of charge movements.[59] The result provides a clear way to design sensitizers with high charge separation efficiency and limited electron recombination. Overall, we find that the adoption of pyrimidyl spacers would make for overall higher fractions of electron exchange and distances of charge transfer, especially in the low energy region, which we are most interested in. The sensitizers

should have strong absorption from the blue end of the visible spectrum to the near infrared. Virtually all of the solar irradiance reaching the earth's surface falls between the wavelengths of 300 and 2500 nm, with roughly half of the available power in the range of 400 to 750 nm.[13,60] The data we provide are all allocated in this region.

4. Conclusion

Comprehensive calculations and parallel comparisons are implemented to interpret the role of that the π-spacer plays in the performance of DSSCs. We pay considerable attention to the comparison between an electron deficient spacer and an electron rich spacer; pyrimidyl and phenyl groups listed here. For phenyl bridged porphyrins, the extension of the π-spacer would reduce the driving force for electron injection and regeneration. Unfavorable charge separations are also obtained for phenyl bridged porphyrins. Calculations on phenyl bridged porphyrins reproduce well the experimental results and help us to understand the role that the phenyl group plays in tuning the PCE. Performances are greatly changed when electron deficient pyrimidyl spacers are adopted. Higher light harvesting efficiency, more advantageous regeneration of oxidized dye and more effective charge separation are acquired, which are integral factors affecting V_{oc}, and J_{sc}, further improving the photo-to-electric efficiency. The extension of pyrimidyl spacer makes further efforts in improving the sensitizer performances. With the extension of π-spacer, more room is provided for modifications of electronic structure, and the process of electron recombination is hindered. So the prototype pyrimidyl bridged porphyrin gives us a successful concept for accommodating more outstanding photo-to-electric conversion efficiency of DSSCs.

Acknowledgements

We acknowledge generous financial support from the National Natural Science Foundation of China (Nos. 21173169 and 20803059) and the Fundamental Research Funds for the Central Universities (No. XDJK2013A008).

Notes and References

1 B. O'Regan and M. Grätzel, *Nature*, 1991, **353**, 737–740.
2 A. Hagfeldt, G. Boschloo, L. C. Sun, L. Kloo and H. Pettersson, *Chem. Rev.*, 2010, **110**, 6595–6663.
3 M. A. Green, K. Emery, Y. Hishikawa and W. Warta, Solar Cell Efficiency Tables (version 37), *Prog. Photovoltaics*, 2011, **19**, 84–92.
4 F. Gao, Y. Wang, D. Shi, J. Zhang, M. Wang, X. Jing, R. Humphry-Baker, P. Wang, S. M. Zakeeruddin and M. Grätzel, *J. Am. Chem. Soc.*, 2008, **130**, 10720–10728.
5 A. Kay and M. Grätzel, *J. Phys. Chem.*, 1993, **97**, 6272–6277.
6 C.-Y. Lin, C.-F. Lo, L.-Y. Luo, H.-P. Lu, C.-S. Hung and E. W.-G. Diau, *J. Phys. Chem. C*, 2009, **113**, 755–764.
7 L.-Y. Luo, C.-J. Lin, C.-S. Hung, C.-F. Lo, C.-Y. Lin and E. W.-G. Diau, *Phys. Chem. Chem. Phys.*, 2010, **12**, 12973–12977.
8 S.-L. Wu, H.-P. Lu, H.-T. Yu, S.-H. Chuang, C.-L. Chiu, C.-W. Lee, E. W.-G. Diau and C.-Y. Yeh, *Energy Environ. Sci.*, 2010, **3**, 949–955.
9 E. M. Barea, G. V. Pedro, T. R. Sanchis, H.-P. Wu, L.-L. Li, C.-Y. Yeh, E. W.-G. Diau and J. Bisquert, *J. Phys. Chem. C*, 2011, **115**, 10898–10902.
10 A. Yella, H.-W. Lee, H. N. Tsao, C.-Y. Yi, A. K. Chandiran, M. K. Nazeeruddin, E. W.-G. Diau, C.-Y. Yeh, S. M. Zakeeruddin and M. Grätzel, *Science*, 2011, **334**, 629–634.
11 R.-X. He, H.-B. Li, W. Shen, Q.-L. Yang and M. Li, *J. Mol. Spectrosc.*, 2012, **275**, 61–70.
12 M.-Y. Guo, R.-X. He, Y.-L. Dai, W. Shen, M. Li, C.-Y. Zhu and S.-H. Lin, *J. Chem. Phys.*, 2012, **136**, 144313–144327.
13 T. W. Hamann, R. A. Jensen, A. B. F. Martinson, H. V. Ryswykac and J. T. Hupp, *Energy Environ. Sci.*, 2008, **1**, 66–78.
14 M. Gouterman, *J. Chem. Phys.*, 1959, **30**, 1139–1261.
15 M. Gouterman, *J. Mol. Spectrosc.*, 1961, **6**, 138–163.
16 M. Gouterman, *J. Mol. Spectrosc.*, 1963, **11**, 108–127.
17 O. V. Prezhdo, W. R. Duncan and V. V. Prezhdo, *Prog. Surf. Sci.*, 2009, **84**, 30–68.
18 A. Listorti, B. O'Regan and J. R. Durrant, *Chem. Mater.*, 2011, **23**, 3381–3399.
19 P. Bonhote, J.-E. Moser, R. Humphry-Baker, N. Vlachopoulos, S. M. Zakeeruddin, L. Walder and M. Grätzel, *J. Am. Chem. Soc.*, 1999, **121**, 1324–1336.
20 N. Hirata, J.-J. Lagref, E. J. Palomares, J. R. Durrant, M. K. Nazeeruddin, M. Grätzel and D. D. Censo, *Chem. Eur. J.*, 2004, **10**, 595–602.
21 J. N. Clifford, E. Palomares, M. K. Nazeeruddin, R. Thampi, M. Grätzel and J. R. Durrant, *J. Am. Chem. Soc.*, 2004, **126**, 5670–5671.
22 M. Alebbi, C. A. Bignozzi, T. A. Heimer, G. M. Hasselmann and G. J. Meyer, *J. Phys. Chem. B*, 1998, **102**, 7577–7581.
23 I. Montanari, J. Nelson and J. R. Durrant, *J. Phys. Chem. B*, 2002, **106**, 12203–12210.
24 J. Wiberg, T. Marinado, D. P. Hagberg, L.-C. Sun, A. Hagfeldt and B. Albinsson, *J. Phys. Chem. B*, 2010, **114**, 14358–14363.
25 J. N. Clifford, E. Palomares, M. K. Nazeeruddin, M. Grätzel, J. Nelson, X. Li, N. J. Long and J. R. Durrant, *J. Am. Chem. Soc.*, 2004, **126**, 5225–5233.
26 M. Myahkostupov, P. Piotrowiak, D. Wang and E. Galoppini, *J. Phys. Chem. C*, 2007, **111**, 2827–2829.
27 D. Wang, R. Mendelsohn, E. Galoppini, P. G. Hoertz, R. A. Carlisle and G. J. Meyer, *J. Phys. Chem. B*, 2004, **108**, 16642–16653.
28 M.-Y. Guo, R.-X. He, Y.-L. Dai, W. Shen, M. Li, C.-Y. Zhu and S.-H. Lin, *J. Phys. Chem. C*, 2012, **116**, 9166–9179.
29 D. Jacquemin, E. A. Perpete, I. Ciofini and C. Adamo, *Acc. Chem. Res.*, 2009, **42**, 326–334.
30 D. Jacquemin, V. Wathelet, E. A. Perpete and C. Adamo, *J. Chem. Theory Comput.*, 2009, **5**, 2420–2435.
31 A. J. Cohen, P. M. Sanchez and W.-T. Yang, *Chem. Rev.*, 2012, **112**, 289–320.
32 J. Zhang, H.-B. Li, S.-L. Sun, Y. Geng, Y. Wu and Z.-M. Su, *J. Mater. Chem.*, 2012, **22**, 568–576.

33 S. Agrawal, P. Dev, N. J. English, K. R. Thampi and J. M. D. MacElroy, *Chem. Sci.*, 2012, **3**, 416–424.
34 M. E. Casida, C. Jamorski, K. C. Casida and D. R. Salahub, *J. Chem. Phys.*, 1998, **108**, 4439–4450.
35 A. Rosa, G. Ricciardi, E. J. Baerends and S. J. A. van Gisbergen, *J. Phys. Chem. A*, 2001, **105**, 3311–3327.
36 C. J. Cramer, *Essentials of Computational Chemistry-Theories and Models*, John Wiley & Sons: Ltd., New York, 2002, pp. 252–253.
37 S. Fantacci, F. De Angelis and A. Selloni, *J. Am. Chem. Soc.*, 2003, **125**, 4381–4387.
38 P. Persson and J. L. Maria, *J. Phys. Chem. B*, 2005, **109**, 11918–11924.
39 J. Muscat, A. Wander and N. M. Harrison, *Chem. Phys. Lett.*, 2001, **342**, 397–401.
40 P. Persson, J. C. M. Gebhardt and S. Lunell, *J. Phys. Chem. B*, 2003, **107**, 3336–3339.
41 F. De Angelis, A. Tilocca and A. Selloni, *J. Am. Chem. Soc.*, 2004, **126**, 15024–15025.
42 A. Dreuw and M. Head-Gordon, *J. Am. Chem. Soc.*, 2004, **126**, 4007–4016.
43 A. Dreuw, J. L. Weisman and M. J. Head-Gordon, *J. Chem. Phys.*, 2003, **119**, 2943–2946.
44 D. Jacquemin, E. A. Perpete, G. E. Scuseria, I. Ciofini and C. Adamo, *J. Chem. Theory Comput.*, 2008, **4**, 123–135.
45 D. Casanova, F. P. Rotzinger and M. Grätzel, *J. Chem. Theory Comput.*, 2010, **6**, 1219–1227.
46 N. H. List, J. M. Olsen, T. Rocha. Rinza, O. Christiansen and J. Kongsted, *Int. J. Quantum Chem.*, 2012, **112**, 789–800.
47 T. Lu and F.-W. Chen, *J. Comput. Chem.*, 2012, **33**, 580.
48 T. L. Bahers, C. Adamo and I. Ciofini, *J. Chem. Theory Comput.*, 2011, **7**, 2498–2506.
49 M. J. Frisch, G. W. Trucks, H. B. Schlegel, G. E. Scuseria, M. A. Robb, J. R. Cheeseman, G. Scalmani, V. Barone, B. Mennucci, G. A. Petersson, H. Nakatsuji, *et al.*, *Gaussian 09, Revision A.01*, Gaussian, Inc., Wallingford, CT, 2009.
50 J. Preat, C. Michaux, D. Jacquemin and E. A. Perpete, *J. Phys. Chem. C*, 2009, **113**, 16821–16833.
51 G. Schlichthorl, N. G. Park and A. J. Frank, *J. Phys. Chem. B*, 1999, **103**, 782–791.
52 I. Ciofini, T. L. Bahers, C. Adamo, F. Odobel and D. Jacquemin, *J. Phys. Chem. C*, 2012, **116**, 11946–11955.
53 J. Wang, F.-Q. Bai, B.-H. Xia, L. Feng, H.-X. Zhang and Q.-J. Pan, *Phys. Chem. Chem. Phys.*, 2011, **13**, 2206–2213.
54 K. Hara, Z.-S. Wang, T. Sato, A. Furube, R. Katoh, H. Sugihara, Y. Dan-Oh, C. Kasada, A. Shinpo and S. Suga, *J. Phys. Chem. B*, 2005, **109**, 15476–15482.
55 Y. Ooyama, Y. Shimada, Y. Kagawa, Y. Yamada, I. Imae, K. Komaguchi and Y. Harima, *Tetrahedron Lett.*, 2007, **48**, 9167–9170.
56 M. K. Nazeeruddin, A. Kay, I. Rodicio, R. Humphry-Baker, E. Mueller, P. Liska, N. Vlachopoulos and M. Grätzel, *J. Am. Chem. Soc.*, 1993, **115**, 6382–6390.
57 S. Eu, S. Hayashi, T. Umeyama, Y. Matano, Y. Araki and H. Imahori, *J. Phys. Chem. C*, 2008, **112**, 4396–4405.
58 K. Pettersson, J. Wiberg, T. Ljungdahl, J. Mårtensson and B. Albinsson, *J. Phys. Chem. A*, 2006, **110**, 319–326.
59 J. Wiberg, L.-J. Guo, K. Pettersson, D. Nilsson, T. Ljungdahl, J. Mårtensson and B. Albinsson, *J. Am. Chem. Soc.*, 2007, **129**, 155–163.
60 Report of the Basic Energy Sciences Workshop on Solar Energy Utilization, US Department of Energy, Washington DC, April 18–21, 2005.

